Arch. Metall. Mater. **66** (2021), 2, 443-450

DOI: 10.24425/amm.2021.135877

Ş. ŢĂLU[1*], S. KULESZA[2], M. BRAMOWICZ[3], K. STĘPIEŃ[4], D. DASTAN[5]

ANALYSIS OF THE SURFACE MICROTEXTURE OF SPUTTERED INDIUM TIN OXIDE THIN FILMS

The present research work involves the study of the 3-D surface microtexture of sputtered indium tin oxide (ITO) prepared on glass substrates by DC magnetron at room temperature. The samples were annealed at 450°C in air and were distributed into five groups, dependent on ambient combinations applied, as follows: I group, using argon (Ar); II group, using argon with oxygen ($Ar+O_2$); III group, using argon with oxygen and nitrogen ($Ar+O_2+N_2$); IV group, using argon with oxygen and hydrogen ($Ar+O_2+H_2$); and V group, using argon with oxygen, nitrogen, and hydrogen ($Ar+O_2+N_2+H_2$). The characterization of the ITO thin film surface microtexture was carried out by atomic force microscopy (AFM). The AFM images were stereometrically quantitatively analyzed to obtain statistical parameters, by ISO 25178-2: 2012 and ASME B46.1-2009. The results have shown that the 3-D surface microtexture parameters change in accordance with different fabrication ambient combinations.

Keywords: AFM, DC magnetron sputtering, ITO thin films, stereometric analysis, 3-D surface microtexture

1. Introduction

Thin films made of transparent conducting oxides (TCO) have gained increasing attention in recent years as they provide significant electrical conductivity together with high transparency in the visible range. A wide range of various semiconducting metal oxides has been studied so far, for example, zinc oxide, tin oxide, indium tin oxide (ITO), etc., each of which exhibited a unique combination of extraordinary functional properties [1,2].

Among them, however, ITO was found the most promising candidate for base material in future photoelectric devices, especially flexible ones, because of the progress in the preparation techniques and overall stability of electrical characteristics [3,4].

ITO is a degenerate wide bandgap semiconductor (E_g around 4 eV) with dominant electron conductivity, hence it hardly absorbs visible light. In its crystalline form planar ITO thin films serve as active coatings of optoelectronic devices such as: light-emitting diodes [5], solar cells [6,7], flat panel displays [8], low-emissivity layers in the infrared range [9], etc., with the overall performance improved compared to other TCOs.

Nowadays, several different methods were demonstrated to perform successful deposition of ITO thin films, including: sol-gel method [10], chemical solution deposition [11], electron beam evaporation [12], physical vapor deposition [13] and magnetron sputtering [14].

Among them, it is the DC magnetron sputtering which appears the most profitable in industrial technology. Several deposition parameters, such as substrate temperature, power supply, and the actual composition of the gas mixture, are the key factors that influence the quality of the deposited material [15].

Usually, chemically inert argon atoms, which are abundant in the ambient atmosphere in the process chamber, are mixed with other gaseous species: oxygen, hydrogen and nitrogen [16-21].

Changes in structural and morphological properties of ITO films grown from various gas mixtures were extensively studied. Wan et al. prepared ITO films using argon with oxygen or hydrogen and they attained the (222) and (400) planes, respectively [22]. Likewise, deposition from nitrogen-enriched argon gas mixture resulted in ITO films with predominant (222) orientation [23]. Similar to crystalline properties, morphology and surface geometry of ITO thin films appear to be strongly influenced by the chemical species present in the process atmosphere [14].

Several papers on nanometric characteristics of planar ITO films deposited by RF magnetron sputtering have been published

[1] TECHNICAL UNIVERSITY OF CLUJ-NAPOCA, THE DIRECTORATE OF RESEARCH, DEVELOPMENT AND INNOVATION MANAGEMENT (DMCDI), CLUJ-NAPOCA, 400020, ROMANIA
[2] UNIVERSITY OF WARMIA AND MAZURY IN OLSZTYN, FACULTY OF TECHNICAL SCIENCES, 11 OCZAPOWSKIEGO STR., 10-719 OLSZTYN, POLAND
[3] UNIVERSITY OF WARMIA AND MAZURY IN OLSZTYN, FACULTY OF TECHNICAL SCIENCES, 11 OCZAPOWSKIEGO STR., 10-719 OLSZTYN, POLAND
[4] KIELCE UNIVERSITY OF TECHNOLOGY, FACULTY OF MECHATRONICS AND MECHANICAL ENGINEERING, ALEJA 1000-LECIA PAŃSTWA POLSKIEGO 7, 25-314 KIELCE, POLAND
[5] GEORGIA INSTITUTE OF TECHNOLOGY, SCHOOL OF MATERIALS SCIENCE AND ENGINEERING, ATLANTA, GEORGIA 30332, USA

* Corresponding author: stefan_ta@yahoo.com

yet. For example, Nie et al. [24] studied the role of argon-based atmosphere upon addition of oxygen and hydrogen molecules, while Jagar et al. [25] reported morphological properties of the hydrogenated indium oxide films deposited using water vapour or hydrogen by sputtering method. Research works on the morphology of ITO films on various substrates, such as: glass, silicon of different crystallinity etc., were carried out as well providing detailed microstructural characteristics of the deposited layers in terms of crystallite size, granular structure and so on [26]. According to previous findings, the key factors that determine fundamental performance of the optoelectronic devices, are the microstructure and morphology of their basal material. To deal with that issue, Korobov, et al. discussed various growth modes, film's continuity etc. of the ITO films on glass substrates [27].

Early growth stages of similar structures deposited by DC magnetron sputtering were analyzed by Shigesato et al. [28], while switching between spatial and planar growth regimes of ITO layers was studied by others [28,29].

Among other experimental methods, Atomic Force Microscopy (AFM) technique is found especially helpful in studying geometrical characteristic of surfaces of the solids at various scales and in different aspects [30-33]. AFM maps a surface under study through sampling forces acting on a sharp tip stuck to the end of elastic cantilever, which remains in permanent or intermittent contact with the surface. Having height samples in the form of a data series, several different methods are possible to describe peculiarities of the surface geometry using, for example statistical parameters. However, statistical quantities suffer from ambiguity, which means that different surface textures expressed as a sequence of data entries can exhibit similar probability distributions making any investigation highly speculative and unclear. On the other hand, fractal analysis, which makes use of the allometric scaling, allows to unveil complex surface geometries in terms of possible alignment patterns and/or long-range orders [34-37]. Among many others, fractal characteristics of ITO films annealed at various temperatures were studied by Raoufi, et al. [38] who also correlated obtained fractal dimension with specific features of surface morphology.

Apart from that, Ţălu et al. [39] studied the fractal nature of the DC magnetron sputtered ITO thin films grown from various argon-based gas mixtures in connection with their structural properties seen through X-ray Diffraction (XRD). This research is related to both: modern materials for electronics and modern research technique – AFM.

In the present study the growth modes of ITO films sputtered in modified process atmospheres were examined using AFM methods and the observed morphology and grain sizes of the films were discussed in terms of chemical components of the gas mixture. Overall spatial characteristics of surfaces of the ITO thin films were studied using fractal approach, whereas their morphological properties were examined using stereometric analysis.

2. Experimental

2.1. Materials

In_2O_3/SnO_2 (90% / 10%) target, corning glass (VWR) substrate, argon (Ar), oxygen (O_2), nitrogen (N_2), and hydrogen (H_2), Methanol and DI-Water.

2.2. Methods

2.2.1. ITO deposition and annealing

ITO films were deposited on glass substrates (Corning supplied by VWR International) using DC magnetron sputtering method at room temperature. Prior to the process the substrates were ultrasonically cleaned in methanol and DI water followed by drying in nitrogen stream. Five samples of ITO films were prepared from gas mixtures containing various amounts of reactive species corresponding to their absolute flows, namely: M1 – Ar (180 sccm), M2 – Ar/O_2 (180/10 sccm), M3 – $Ar/O_2/N_2$ (180/10/10 sccm), M4 – $Ar/O_2/H_2$ (180/10/10 sccm) and M5 – $Ar/O_2/N_2/H_2$ (180/10/10/10 sccm). The vacuum chamber was evacuated down to 10^{-7} mbar to obtain base pressure, but kept at 3.1×10^{-3} mbar when preceded with the deposition process. Obtained ITO films were then annealed for 1 hour at 450°C in an ambient atmosphere.

2.2.2. AFM measurements

Surface geometry of the films was investigated by means of Atomic Force Microscopy using Dimension 3000 instrument (Veeco). Height samples were taken at the nodes of a discrete raster grid with lateral resolution 512 points by processing transient phase shifts in damped oscillations of a silicon cantilever (Budget Sensors Tap300Al-G) relative to driving force generated by the piezo. Square AFM images with the length 2 μm were scanned at a rate 0.55 Hz per line maintaining amplitude setpoint 1.1 V.

2.3. Multiaspect surface microtexture analyses based on AFM data

AFM images provide height samples $z(x,y)$ of the surface under study span over square raster grid. In order to determine the 3-D surface morphology and to obtain various statistics of the surface texture at the micrometric level, AFM data were processed using SPIP^{TM} 6.7.4 software, according to ISO 25178-2: 2012 and ASME B46.1-2009. In all the measurements, two areas of each sample were scanned, analyzed and compared based on their 3-D surface texture characteristics.

2.4. Statistical analysis

Statistical analysis on the AFM images was performed using the SPSS 14 for Windows (Chicago, Illinois, USA). One way analysis of variance (ANOVA) was used to test the differences between the two groups with Scheffé post hoc tests for multiple comparisons. Differences with a P value of 0.05 or less were considered statistically significant.

3. Results and discussion

3.1. Fractal analysis

Fig. 1 presents AFM images of the samples under investigation probed with the scan length 2 μm and lateral resolution 512 points per line. In general, deposited ITO films reveal regular structure with well-developed grains, but their specific

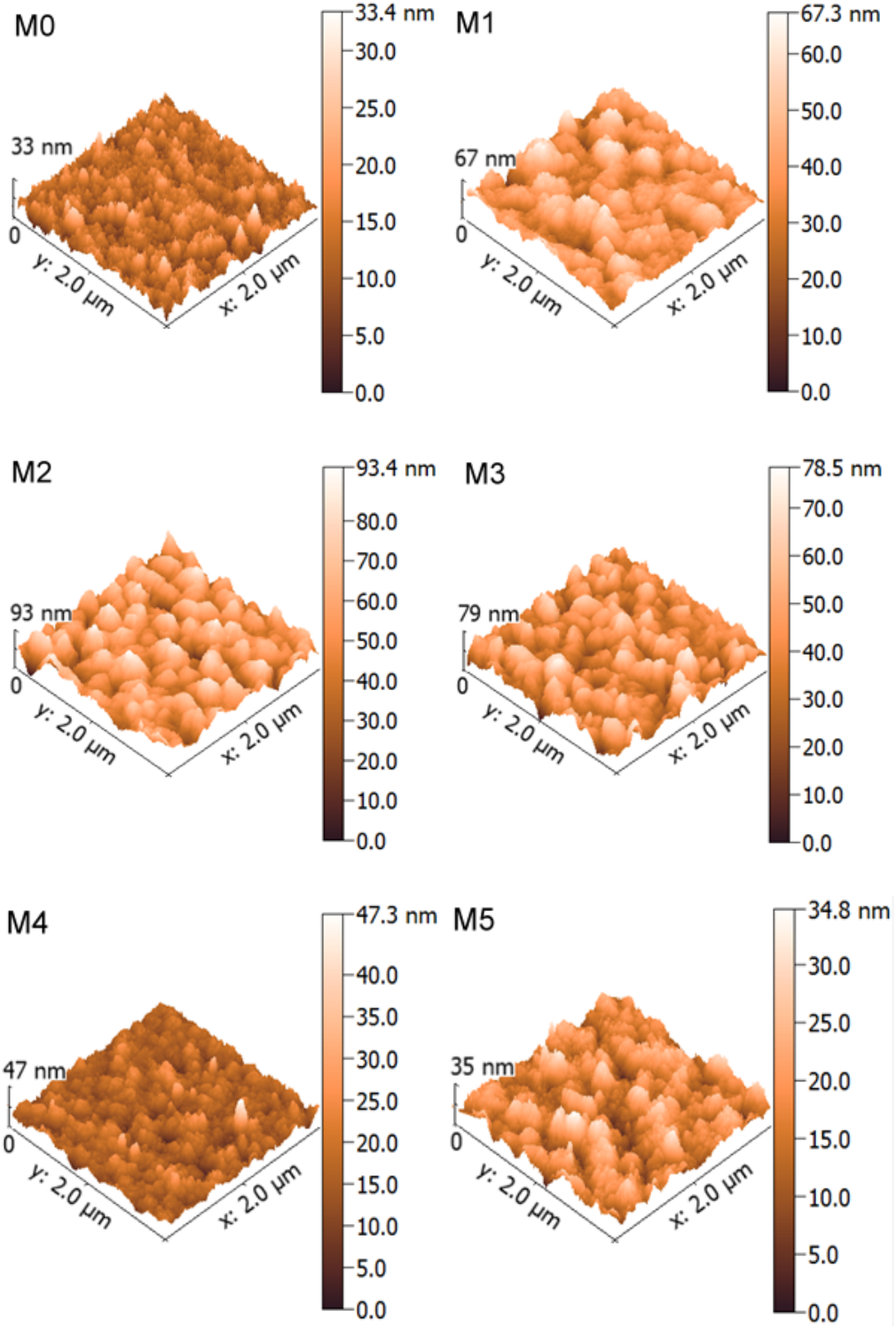

Fig. 1. AFM images of the ITO thin films with the scan length 2 μm: M0 – reference sample, M1 sample, M2 sample, M3 sample, M4 sample, M5 sample

surface texture characteristics lie on a spectrum depending on the process details. Table 1 summarizes spatial characteristics of these surfaces determined using statistical measures, while Table 2 provides fractal parameters derived via allometric scaling approach. A comparison of results obtained for various ITO samples shows several correspondence patterns, which might have their roots in the roles the gaseous species play in the deposition process. The following samples appear similar in that aspect: reference with M4, M2 with M3, and M1 with M5.

The height histograms (gray lines) with their respective cumulative distribution curves (red lines) obtained from AFM images (Fig. 1) are plotted in Fig. 2.

Fig. 3 shows respective material curves obtained from AFM images in Fig. 1.

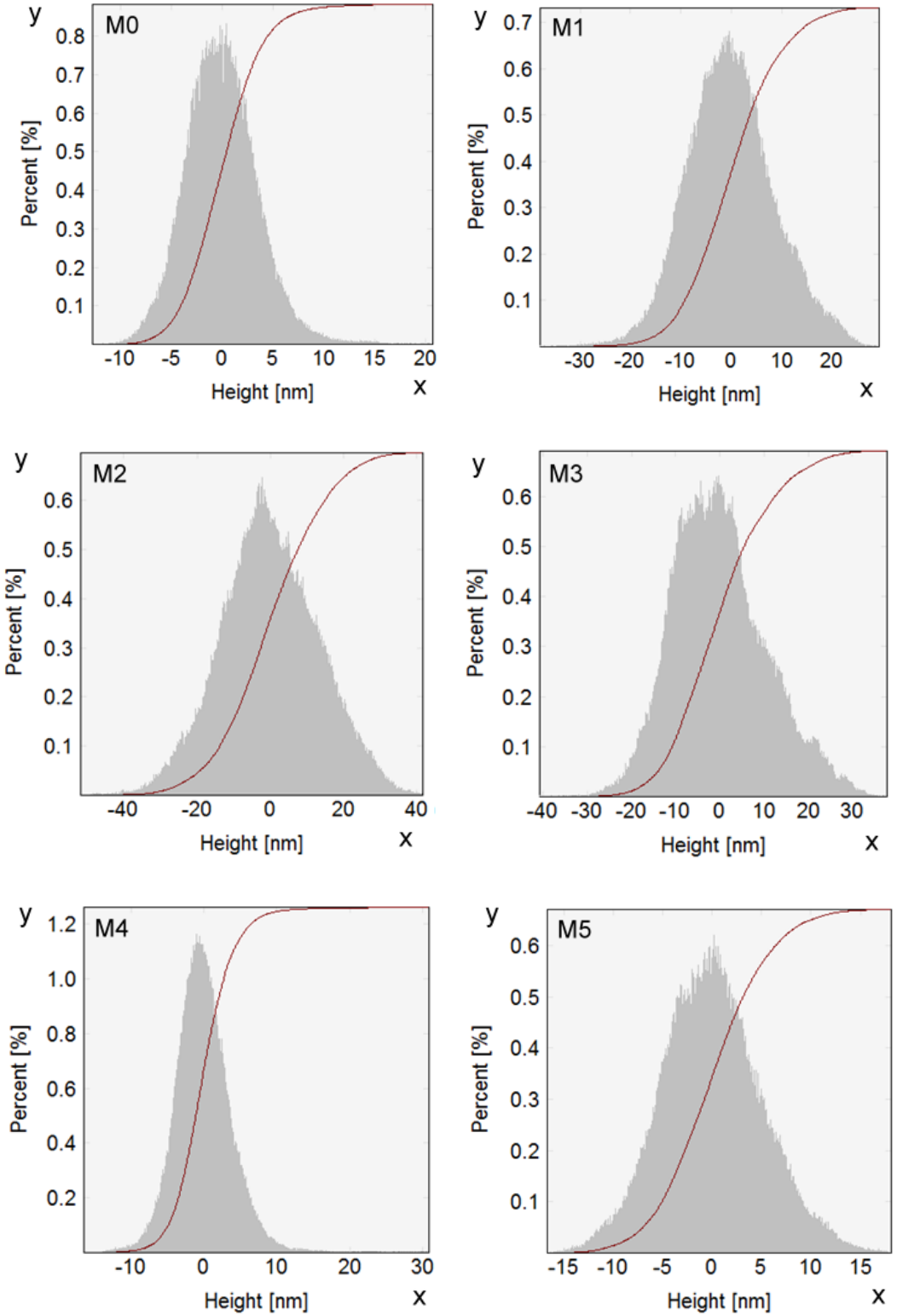

Fig. 2. The height data histograms (gray) and respective cumulative distribution curves (red) obtained from AFM data of the samples under investigation

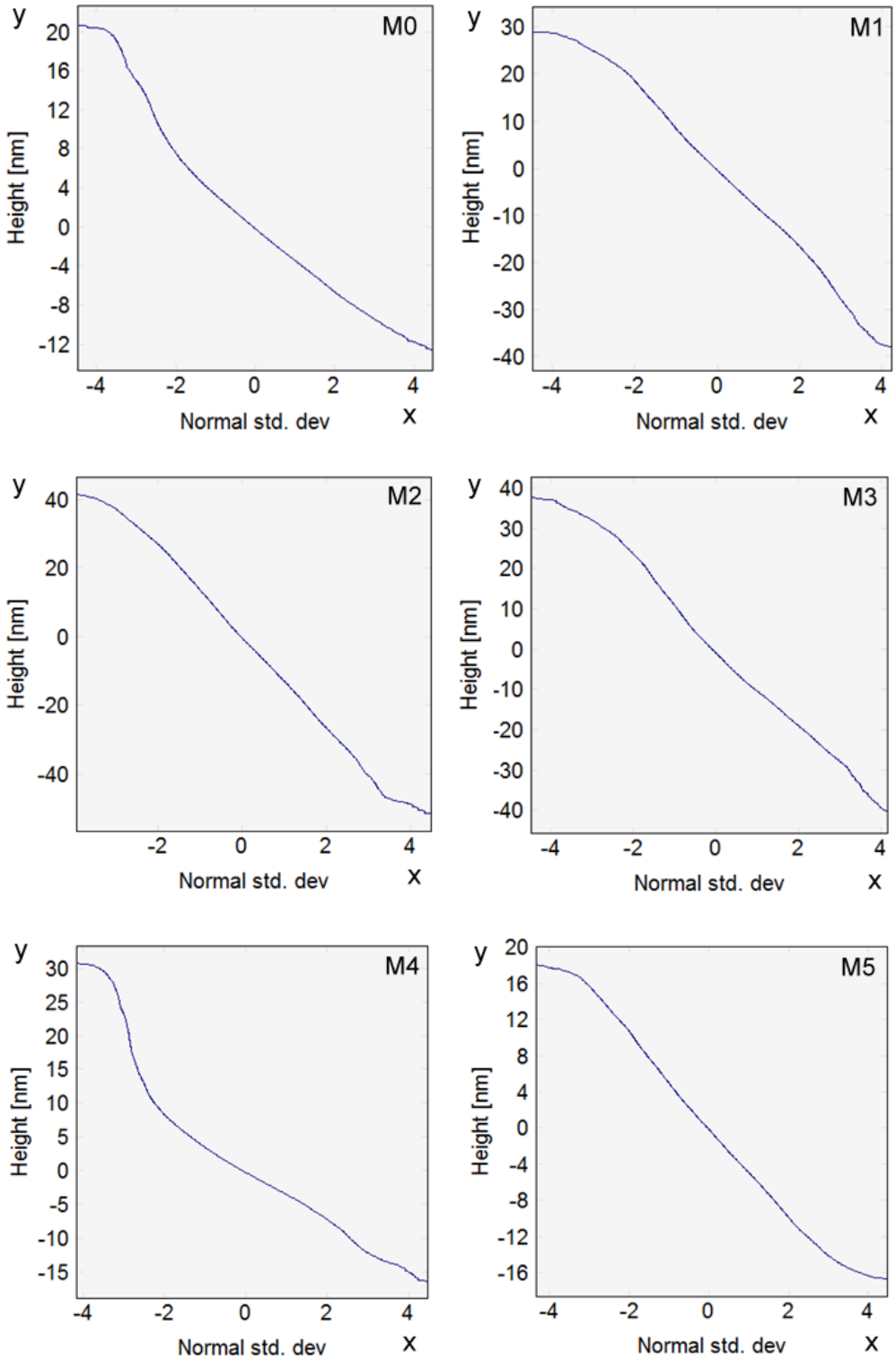

Fig. 3. Material curve plots obtained from AFM images

Fig. 4 presents plots of respective angular spectra of AFM images in Fig. 1. The angular spectrum is a radial plot of relative amplitudes revealing predominant orientation of the surface texture. Each relative amplitude is found as a sum of all amplitudes along given radial line in the Fourier spectrum of AFM image

Specific characteristics of the surface texture seen in AFM images were derived according to ISO 25178-2: 2012 and ASME B46.1-2009 (Table 1).

Table 2 presents data that demonstrates direct dependence between chemical composition of the gas mixture used throughout the process and surface texture of deposited materials, which in turn reflects their internal structure. First of all, the grain size d_{grain} is found to be around 50-80 per cent larger compared to the corner frequency τ_c. Such inequality might be due to the fact that the particles itself appear nearly identical in size and shape, but they are spread over the surface in a random manner not giving

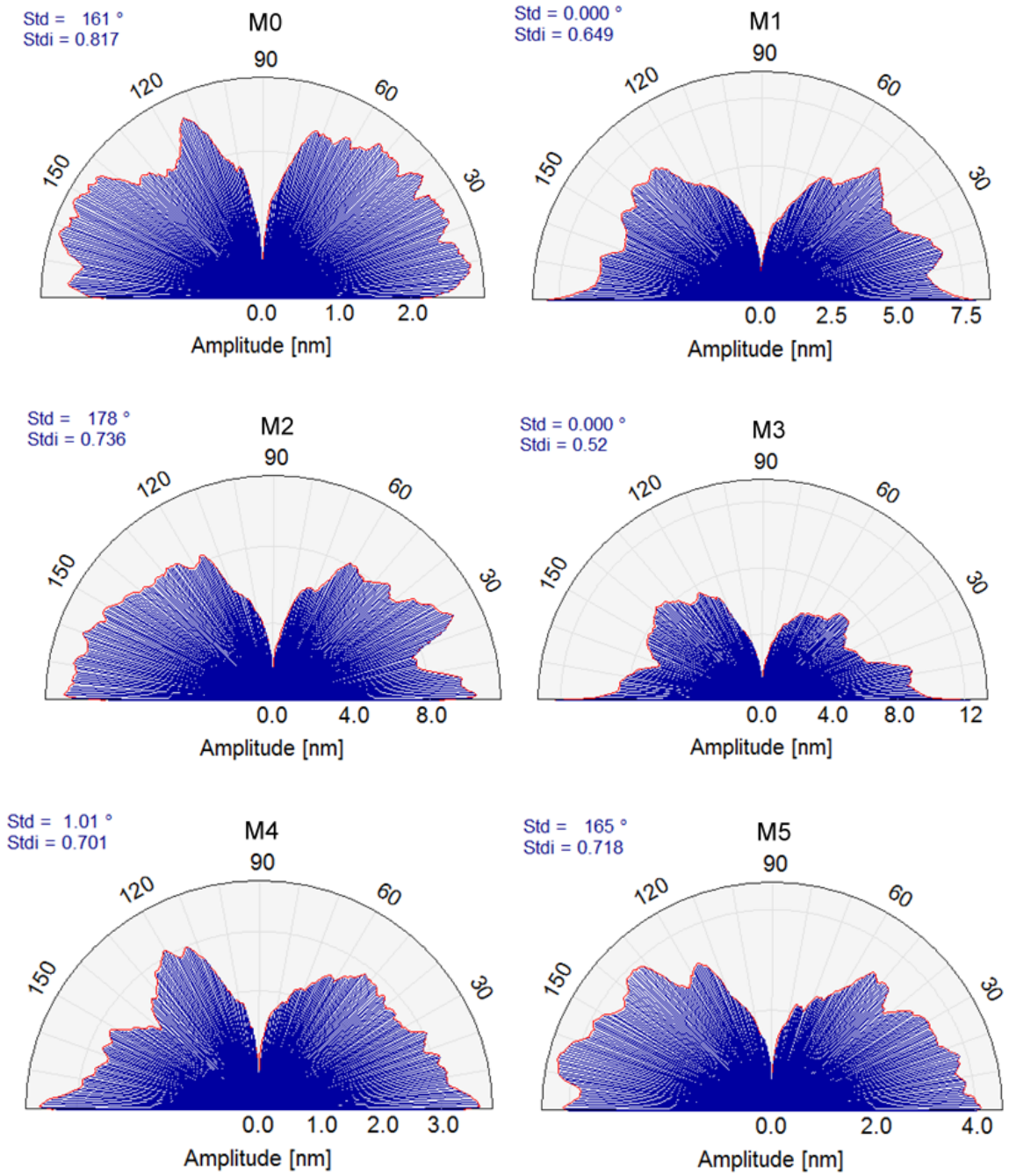

Fig. 4. Angular spectra of the samples under study derived from respective AFM images

rise to any long-range order. Particles grown from pure argon (M1) reach 220 nm in their diameter, that is double the size in the reference sample (M0). Similar to the latter, however, these particles turn out to have subgranular, regular structure with grains 70-80 nm in diameter spread homogeneously over the surface. In CVD processes of diamond deposition argon particles are found responsible for enhanced formation of nanocrystalline phase because of higher concentration of free electrons in the gas mixture, and hence the intense creation of nucleation centers on the surface [39]. The grain size can be further decreased to 170 nm when molecular oxygen is added to the gas mixture (sample M2). Similar effect was observed upon addition of molecular nitrogen (sample M3), which means that this gas makes no influence on the crystalline structure of the deposits. On the other hand, the substitution of nitrogen molecules for those of hydrogen (sample M4) results in a structure very close to that in the reference sample in terms of the grain size and spatial characteristics of surface geometry. One can therefore conclude that oxygen and hydrogen molecules in the gas mixture act cooperatively towards nanocrystalline phase. High anisotropy ratio (S_{tr} equal to 0.71) follows from fine-grain structure of this film, without any larger clusters. Unlike M4, however, M5 grown from the quaternary gas mixture appears coarse-grain structure with 200 nm particles and moderate anisotropy. Mutual interactions between gaseous species in the gas phase are supposed to suppress overall nucleation density.

TABLE 1

Multi-aspect surface texture statistics derived from AFM images according to ISO 25178-2: 2012 and ASME B46.1-2009

Statistical parameter	Symbol	Samples					
		M0	M1	M2	M3	M4	M5
Amplitude Parameters							
Arithmetic mean height	Sa [nm]	2.7	6.8	10.5	8.4	2.9	3.9
Root mean square height	Sq [nm]	3.5	8.6	13.3	10.6	3.9	5.0
Surface skewness	Ssk [-]	0.46	0.13	0.01	0,37	0.85	0.15
Surface kurtosis	Sku [-]	4.13	3.14	2.93	2.99	7.28	3.05
Maximum height	Sz [nm]	33.4	67.3	93.4	78.5	47.2	34.7
Ten-point height	S10z [nm]	28.9	62.6	88.7	68.7	41.2	33.3
Maximum valley depth	Sv [nm]	12.7	37.9	51.7	40.7	16.4	16.6
Maximum peak height	Sp [nm]	20.7	29.3	41.6	37.8	30.84	18.1
Hybrid Parameters							
Mean Summit Curvature	Ssc [1/nm]	0.1166	0.1096	0.2691	0.1149	0.0874	0.0812
Root mean square gradient	Sdq [-]	0.3133	0.3708	0.6165	0.4514	0.2871	0.2716
Area Root Mean Square Slope	Sdq6	0.2972	0.3549	0.5891	0.4365	0.2717	0.2585
Surface area ratio	Sdr [%]	4.607	6.336	15.65	8.966	3.766	3.418
Projected Area	S2A [nm²]	4E+06	4E+06	4E+06	4E+06	4E+06	4E+06
Surface Area	S3A [nm²]	4.1E+06	4.2E+06	4.6E+06	4.3E+06	4.1E+06	4.1E+06
Functional Parameters							
Surface Bearing Index	Sbi	0.2364	0.6039	0.6953	0.5846	0.1597	0.529
Core Fluid Retention Index	Sci	1.613	1.677	1.618	1.807	1.603	1.65
Valley Fluid Retention Index	Svi	0.1021	0.1046	0.112	0.0907	0.1029	0.1074
Reduced Summit Height	Spk [nm]	5.1	10.0	13.4	13.1	6.2	5.7
Core Roughness Depth	Sk [nm]	8.7	21.4	32.9	26.5	8.6	12.6
Reduced Valley Depth	Svk [nm]	2.8	7.5	12.7	7.6	3.5	4.3
Spatial Parameters							
Density of summits	Sds [μm^{-2}]	1291	875	513.3	512.8	914	808.8
Texture direction	Std [°]	161.4	0	177.7	0	1.006	165.1
Texture direction index	Stdi [-]	0.8165	0.6486	0.7362	0.52	0.701	0.7181
Dominant radial wavelength	Srw [nm]	422.4	588	481.5	502.6	455.2	626.7
Radial wave index	Srwi [-]	0.0608	0.0289	0.0428	0.0451	0.0488	0.0367
Mean half wavelength	Shw [nm]	181.8	333.3	250	285.7	200	285.7
Correlation length at 20%	Scl20 [nm]	66.5	109.6	82.1	93.9	74.3	93.9
Correlation length at 37%	Scl37 [nm]	50.8	90.0	66.5	74.3	58.7	74.3
Texture-aspect ratio at 20%	Str20 [-]	0.7391	0.6667	0.6364	0.6667	0.7037	0.5854
Texture-aspect ratio at 37%	Str37 [-]	0.7647	0.697	0.6538	0.7308	0.7895	0.6786
Cross hatch angle	Sch [°]	46.55	67.66	48.99	48.14	58.83	29.33

* Statistically significant difference for all values: $P < 0.05$.

TABLE 2

Correlational and scale-invariant surface texture characteristics derived from AFM images

Statistical parameter	Symbol	Samples					
		M0	M1	M2	M3	M4	M5
Anisotropy ratio	S_{tr} [-]	0.72	0.65	0.62	0.70	0.71	0.58
Fractal dimension	D [-]	2.42	2.34	2.31	2.30	2.39	2.35
Corner frequency	τ_c [nm]	70	130	110	100	80	110
Grain diameter	d_{grain} [nm]	110	220	170	170	120	200

4. Conclusions

Demonstrated influence exerted by active gaseous species present in the process atmosphere on ITO specimens provide insight into better understanding of material properties in terms of their future applications. Multi-aspect spatial characteristics of surface micromorphology combined with fractal analysis offer reliable assessment tool for optimization of structural properties of ITO films on various substrates. Morphological features of the deposits either on local or global scales can be effectively characterized using minimal set of unique parameters.

Acknowledgments

The authors would like to thank to Professor Joshua M. Pearce, and Adam Pringle (Department of Materials Science & Engineering, Michigan Technological University, Houghton, MI 49931-1295, USA), for providing AFM data.

REFERENCES

[1] V.A. Dao, H. Choi, J. Heo, H. Park, K. Yoon, Y. Lee, Y. Kim, N. Lakshminarayan, J. Yi, Curr. Appl. Phys. **10** (3), S506-S509 (2010). DOI: 10.1016/j.cap.2010.02.019

[2] B. Zhang, N.N. Zhang, J.F. Chen, Y. Hou, S. Yang, J.W. Guo, X.H. Yang, J.H. Zhong, H.F. Wang, P. Hu, H.J. Zhao, H.G. Yang, Sci. Rep. **3**, 3109 (2013). DOI: 10.1038/srep03109

[3] O.M. Livvik, S. Diplas, A. Romanyuk, A. Ulyashin, J. Appl. Phys. **115**, 083705 (2014). DOI: 10.1063/1.4866991

[4] A.J. Freeman, K.R. Poeppelmeier, T.O. Mason, R.P.H. Chang, T.J. Marks, MRS Bulletin. **25** (8), 45-51 (2000). DOI: 10.1557/mrs2000.150

[5] Q. Wan, E.N. Dattoli, W.Y. Fung, W. Guo, Y. Chen, X. Pan, W. Lu, Nano Lett. **6** (12), 2909-2915 (2006). DOI: 10.1021/nl062213d

[6] L. Shui-Yang, Thin Solid Films. **42** (8), S10-S13 (2010). DOI: 10.1016/j.tsf.2010.03.023

[7] J.H. Noh, H.S. Han, S. Lee, J.Y. Kim, K.S. Hong, G.-S. Han, H. Shin, H.S. Jung, Adv. Energy Mater. **1** (5), 829-835 (2011). DOI: 10.1002/aenm.201100241

[8] N. Boulanger, D.R. Barbero, Appl. Phys. Lett. **103** (2), 021116 (2013). DOI: 10.1063/1.4813498

[9] K. Sun, W. Zhou, X. Tang, F. Luo, Infrared Physics and Technology **78**, 156-161 (2016). DOI: 10.1016/j.infrared.2016.07.021

[10] H. Cho, Y.H. Yun, Ceram. Int. **37** (2), 615-619 (2011). DOI: 10.1016/j.ceramint.2010.09.033

[11] J. Lee, S. Lee, G. Li, M.A. Petruska, D.C. Paine, S. Sun, J. Am. Chem. Soc. **134** (32), 13410-13414 (2012). DOI: 10.1021/ja3044807

[12] M. Himmerlich, M. Koufaki, Ch. Mauder, G. Ecke, V. Cimalla, J.A. Schaefer, E. Aperathitis, S. Krischok, Surf. Sci. **601** (18), 4082-4086 (2007). DOI: 10.1016/j.susc.2007.04.061

[13] V. Vasu, A. Subrahmanyam, Semicond. Sci. Technol. **7** (3), 320 (1992). DOI: 10.1088/0268-1242/7/3/006

[14] I. Hotovy, J. Pezodlt, M. Kadlecikova, T. Kups, L. Spiess, J. Breza, E. Sakalauskas, R. Goldhahn, V. Rehacek, Thin Solid Films. **518** (16), 4508-4511 (2010). DOI: 10.1016/j.tsf.2009.12.018

[15] R. Bel Hadj Tahar, T. Ban, Y. Ohya, Y. Takahashi, J. Appl. Phys. **83**, 2631-2645 (1998).

[16] K. Kato, H. Omoto, T. Tomioka, A. Takamatsu, Thin Solid Films. **520** (1), 110-116 (2011). DOI: 10.1016/j.tsf.2011.06.061

[17] T. Koida, H. Fujiwara, M. Kondo, Solar Energy Materials & Solar cells. **93** (6-7), 851-854 (2009).

[18] D. Dastan, Appl. Phys. A. **123**, 699, 1-13, (2017). DOI: 10.1007/s00339-017-1309-3

[19] D. Dastan, J. Atomic, Molecul., Condensate Nano Phys. (JAMC-NP). **2** (2), 109-114 (2015).

[20] D. Dastan, S. Leila Panahi, A.P. Yengantiwar, A.G. Banpurkar, Adv. Sci. Lett. **22** (4), 950-953 (2016). DOI: 10.1166/asl.2016.7130

[21] M. Marikkannan, M. Subramanian, J. Mayandi, M. Tanemura, V. Vishnukanthan, J.M. Pearce, AIP Advances. **5**, 017128 (2015). DOI: 10.1063/1.4906566

[22] D. Wan, P. Chen, J. Liang, S. Li, F. Huang, ACS. Appl. Mater. Interfaces. **3** (12), 4751-4755 (2011). DOI: 10.1021/am2012432

[23] C. Guillen, J. Herrero, J. Appl. Phys. **101**, 073514 (2007). DOI: 10.1063/1.2715539

[24] M. Nie, T. Mete, K. Ellmer, J. Appl. Phys. **115**, 154905 (2014). DOI: 10.1063/1.4871810

[25] T. Jäger, Y.E. Romanyuk, S. Nishiwaki, B. Bissig, F. Pianezzi, P. Fuchs, C. Gretener, M. Döbeli, A.N. Tiwari, J. Appl. Phys. **117**, 205301 (2015). DOI: 10.1063/1.4921445

[26] N. Manavizadeh, F.A. Boroumand, E.A. Soleimani, F. Raissi, S. Bagherzadeh, A. Khodayri, M. Amin Rasouli, Thin Solid Films. **517** (7), 2324-2327 (2009). DOI: 10.1016/j.tsf.2008.11.027

[27] V. Korobov, M. Leibovitch, Y. Shapira, Appl. Phys. Lett. **65**, 2290 (1994). DOI: 10.1063/1.112721

[28] Y. Shigesato, R. Koshi-ishi, T. Kawashima, J. Oshako, Vacuum. **59**, 614-621 (2000). DOI: 10.1016/S0042-207X(00)00324-9

[29] Y. Sato, M. Taketomo, N. Ito, Miyamura A., Shigestao Y., Thin Solid Films. **516** (14), 4598-4602 (2008).

[30] Ş. Ţălu, Micro and nanoscale characterization of three dimensional surfaces. Basics and applications. Napoca Star Publishing House, Cluj-Napoca, Romania, (2015).

[31] Ş. Ţălu, S. Stach, A. Mahajan, D. Pathak, T. Wagner, A. Kumar, R.K. Bedi, Surf. Interface Anal. **46** (4), 393-398 (2014). DOI: 10.1002/sia.5492

[32] Ş. Ţălu, S. Stach, S. Valedbagi, R. Bavadi, S.M. Elahi, M. Ţălu, Mater. Sci. Poland. **33** (3), 541-548 (2015). DOI: 10.1515/msp-2015-0086

[33] A. Arman, Ş. Ţălu, C. Luna, A. Ahmadpourian, M. Naseri, M. Molamohammadi, J Mater Sci: Mater Electron. **26**, 9630-9639 (2015). DOI: 10.1007/s10854-015-3628-5

[34] N. Naseri, S. Solaymani, A. Ghaderi, M. Bramowicz, S. Kulesza, Ş. Ţălu, M. Pourreza, S. Ghasemi, RSC Advances. **7**, 12923-12930 (2017). DOI: 10.1039/c6ra28795f

[35] D. Elenkova, J. Zaharieva, M. Getsova, I. Manolov, M. Milanova, S. Stach, Ş. Ţălu, Int. J. Polym. Anal. Charact. **20**, 42-56 (2015). DOI: 10.1080/1023666X.2014.955400

[36] Ş. Ţălu, S. Solaymani, M. Bramowicz, S. Kulesza, A. Ghaderi, S. Shahpouri, S.M. Elahi, J. Mater. Sci: Mater. Electron. **27**, 9272-9277 (2016). DOI: 10.1007/s10854-016-4965-8

[37] Ş. Ţălu, S. Stach, S. Valedbagi, S.M. Elahi, R. Bavadi, Mater. Sci. Pol. **33** (1), 137-143 (2015). DOI: 10.1515/msp-2015-0010

[38] D. Raoufi, Physica B: Condensed Matter. **405** (1), 451-455, (2010). DOI: 10.1016/j.physb.2009.09.005

[39] Ş. Ţălu, S. Kulesza, M. Bramowicz, A.M. Pringle, J.M. Pearce, M. Murugesan, V. Venkatachalapathy, J. Mayandi, Materials Letters. **220**, 169-171 (2018). DOI: 10.1016/j.matlet.2018.03.005